

## Investigation on the effect of vibration frequency on vortex-induced vibrations by section model tests

X.G. Hua<sup>\*</sup>, Z.Q. Chen<sup>a</sup>, W. Chen<sup>b</sup>, H.W. Niu<sup>c</sup> and Z.W. Huang<sup>d</sup>

Wind Engineering Research Center, Key Laboratory for Wind and Bridge Engineering of Hunan Province,  
College of Civil Engineering, Hunan University, Changsha 410082, China

(Received November 10, 2014, Revised January 1, 2015, Accepted January 5, 2015)

**Abstract.** Higher-mode vertical vortex-induced vibrations (VIV) have been observed on several steel box-girder suspension bridges where different vertical modes are selectively excited in turn with wind velocity in accordance with the Strouhal law. Understanding the relationship of VIV amplitudes for different modes of vibration is very important for wind-resistant design of long-span box-girder suspension bridges. In this study, the basic rectangular cross-section with side ratio of  $B/D=6$  is used to investigate the effect of different modes on VIV amplitudes by section model tests. The section model is flexibly mounted in wind tunnel with a variety of spring constants for simulating different modes of vibration and the non-dimensional vertical amplitudes are determined as a function of reduced velocity  $U/fD$ . Two 'lock-in' ranges are observed at the same onset reduced velocities of approximately 4.8 and 9.4 for all cases. The second 'lock-in' range, which is induced by the conventional vortex shedding, consistently gives larger responses than the first one and the  $Sc$ -normalized maximum non-dimensional responses are almost the same for different spring constants. The first 'lock-in' range where the vibration frequency is approximately two times the vortex shedding frequency is probably a result of super-harmonic resonance or the "frequency demultiplication". The main conclusion drawn from the section model study, central to the higher-mode VIV of suspension bridges, is that the VIV amplitude for different modes is the same provided that the  $Sc$  number for these modes is identical.

**Keywords:** suspension bridges; bridge deck; vortex-induced vibrations; wind tunnel tests; section model tests

### 1. Introduction

When flow passes over the bluff body, vortices with equal strength but opposite rotation are shed alternately at both sides of the body. The body is then subject to the transverse lift force with the same frequency with that of the vortex pairs. If the body is elastically mounted, transverse vibration may be caused, particularly if the vortex-shedding frequency coincides with a natural

---

\*Corresponding author, Professor, E-mail: [cexghua@hotmail.com](mailto:cexghua@hotmail.com)

<sup>a</sup> Professor, E-mail: [zqchen@hnu.edu.cn](mailto:zqchen@hnu.edu.cn)

<sup>b</sup> Former graduate student, E-mail: [chenwensunny@163.com](mailto:chenwensunny@163.com)

<sup>c</sup> Senior Engineer, E-mail: [niuhw\\_hd@126.com](mailto:niuhw_hd@126.com)

<sup>d</sup> Ph.D. Candidate, E-mail: [zwhuang213112@gmail.com](mailto:zwhuang213112@gmail.com)

frequency of elastic body. The frequency of vortex-shedding depends on wind speed  $U$ , the cross-sectional shape and sometimes the Reynolds number, and is defined by the non-dimensional Strouhal number  $St=fD/U$  where  $D$  is the body dimension in transverse direction. For cross-section with sharp edges such as bridge decks,  $St$  is independent on Reynolds number. Structures specially liable to vortex-induced vibrations are transmission lines, chimney stackers, masts and towers, suspension bridges and pipelines (Scruton and Flint 1964, Simiu and Scanlan 1996). There have been numerous work carried out on vortex-induced vibration of circular cylinders, as well documented in several reviews (e.g., Bearman 1984, Sarpkaya 2004, Williamson and Govardhan 2004).

Bridge decks are typical bluff bodies and are therefore prone to vortex-induced vibrations when exposed to a natural wind. Wu and Kareem (2012) presented a state-of-the-art review on vortex-induced vibration of bridge decks. Due to the relatively high stiffness for beam bridges and cable-stayed bridges, the vortex-induced vibrations have been observed only for the fundamental vertical or torsional mode in practice. However, a long-span suspension bridge is very flexible such that its bridge deck/stiffening girder has a number of closely-spaced vertical modes of vibration. Many of them will be selectively excited in turn with wind velocity in accordance with the Strouhal law  $St=fD/U$ , with  $D$  being the depth of bridge decks in context of bridge VIV. Actually, higher-mode vertical vortex-induced vibrations have been observed on several steel box-girder suspension bridges under moderate wind (Larsen *et al.* 2000, Li *et al.* 2011). For example, as reported by Larsen *et al.* (2000), the third, the fifth and the sixth vertical modes of the stiffening girder developed vortex-induced vibrations at increasing wind velocity for the Great Belt Bridge.

Generally speaking, the steel box girders in suspension bridges may be considered as a shallow beam commonly with a height less than 4m, and its  $St$  number is about 0.1. Therefore, the onset 'lock-in' velocities for vertical modes with a frequency less than 0.6 Hz are below 25 m/s, which is the upper limit wind velocity for bridges open to traffic. In particular, the vertical modes with a frequency following in the range of 0.2 Hz~0.4 Hz have onset velocity of about 6~12 m/s and are therefore most easily excited by vortex shedding than lower modes. On the other hand, at the same amplitude of vibration, vortex-induced vibration of higher modes produces larger acceleration. As a result, restricting the vibration amplitudes for higher vertical modes is more rigorous than that of lower modes, and worthy of more attention. Understanding and prediction of maximum VIV amplitudes for higher modes is essential for wind-resistant design of long-span suspension bridges.

While both computational fluid dynamics and wind tunnel tests may be used to predict the amplitude of vortex-induced vibration (Barrero-Gil and Fernandez-Arroyo 2013, Borna *et al.* 2013), the most reliable technique currently remains wind tunnel tests (Diana *et al.* 2006). Full aeroelastic model of a suspension bridge is most desirable as it directly provide the 'lock-in' velocities and vibration amplitudes for different vertical modes. However, due to the practical difficulty in reproducing bridge deck details in aeroelastic models as well as the large expense and time involved, section model tests are commonly used in practice.

The higher-mode VIV amplitude is related to vortex-induced lift force, modal frequency,  $Sc$  number and span-wise correlation of lift forces under different modes of vibration. This paper describes the experimental investigation regarding the effect of different vibration modes on VIV amplitudes by using section model test in smooth flow. As the section model is used, the results confine themselves to the two-dimension flow conditions. The rectangular cross-section with side ratio of  $B/D=6$  is adopted and the section model is flexibly mounted in wind tunnel with a variety of spring constants for simulating different modes of vibration and the non-dimensional vertical

amplitudes are obtained at increasing wind velocity. For each test, the mass-damping parameter, namely the Scruton ( $Sc$ ) number, remains constant as much as possible. The  $St$  number as well as the maximum non-dimensional vertical amplitude of the section model obtained for each spring constants are compared.

## 2. Existing method for higher mode's VIV

### 2.1 Mathematical model for VIV

Excessive vortex-induced vibration may cause structural fatigue and also discomfort users, and it is therefore necessary to limit the vibration amplitude. However, despite numerous research efforts, accurate prediction of VIV amplitudes of bridge decks remains a difficult problem; the existing mathematical models are mainly semi-analytical and semi-experimental. Some non-parametric models with powerful ability to model nonlinear features have been also applied to simulate the 'lock-in' phenomenon (Wu and Kareem 2012). In this study, the empirical linear model developed by Simiu and Scanlan in 1986 is chosen to discuss the higher-mode vortex-induced vibrations (Simiu and Scanlan 1996). The cross-wind dimension  $D$  of the cylinder (the box-girder depth in the context of suspension bridges), is taken as characteristic length. The equation of motion of the cylinder during lock-in can be written as

$$m(\ddot{y} + 2\zeta\omega_n\dot{y} + \omega_n^2 y) = \frac{1}{2}\rho U^2 2D \left[ Y_1(K_1) \frac{\dot{y}}{U} + Y_2(K_1) \frac{y}{U} \right] + \frac{1}{4}\rho U^2 (2D) C_L(K_1) \sin(\omega_n t + \varphi) \quad (1)$$

where  $m$  is the cylinder mass per unit length;  $\rho$  is the mass density of air;  $U$  is the wind velocity;  $K_1$ , defined as  $D\omega_n/U$ , is the reduced frequency with  $\omega_n$  being the natural frequency of cylinder;  $Y_1(K_1)$ ,  $Y_2(K_1)$  and  $C_L(K_1)$  describe the aerodynamic damping, aerodynamic stiffness and motion-independent vortex-shedding forces at lock-in, and they are functions of reduced frequency  $K_1$ . By defining the non-dimensional amplitude  $\eta = y/D$ , the steady solution for Eq. (1) can be expressed as

$$|\eta| = \frac{\rho D^2 C_L}{2m \sqrt{(K_0^2 - K_1^2)^2 + (2\gamma K_0 K_1)^2}} \quad (2)$$

$$K_0^2 = K_1^2 - \frac{\rho D^2}{m} Y_2(K_1) \quad (3)$$

$$\gamma = \frac{1}{2K_0} \left[ 2\zeta K_1 - \frac{\rho D^2}{m} Y_1(K_1) \right] \quad (4)$$

By analogy, Eq. (2) may be regarded as the response of single degree-of-freedom (SDOF) system with reduced frequency  $K_0$  and damping ratio of  $\gamma$  under forced sinusoidal excitation with frequency  $K_1$ ; during lock-in,  $K_1$  decreases with wind velocity  $U$  and the maximum vibration amplitude  $\eta$  develops when  $K_1 = K_0$ . One can identify the aerodynamic parameters  $Y_1(K_1)$ ,  $Y_2(K_1)$

and  $C_L(K_1)$  from the experimental  $K_1$ - $\eta$  curve obtained from section model wind tunnel tests. The Simiu-Scanlan model only predicts the maximum amplitude for  $K_1=D\omega_n/U$ , and it cannot also provide the range of wind velocity at lock-in.

The vibration amplitude described by Eqs. (2)-(4) are implicit functions of aerodynamic parameters  $Y_1(K_1)$ ,  $Y_2(K_1)$  and  $C_L(K_1)$ . Substituting Eqs. (3) and (4) into Eq. (2) yields

$$|\eta| = \frac{C_L}{2\sqrt{Y_2^2 + (2K_1^2 S_c - Y_1)^2}} \quad (5)$$

where  $S_c$  is the Scruton number defined as  $S_c=2m\delta/\rho D^2$ .

By letting  $Y_1=Y_2=0$ , Eq. (5) reduces to the case of the most simple linear model of vortex-shedding forces considering only the motion-independent term. In such case, the solution of VIV amplitude reduces to

$$|\eta|_L = \frac{C_L}{16\pi^2 S_t^2 S_c} \quad (6)$$

where  $|\eta|_L$  represents the solution of SDOF system for the simple linear model of vortex shedding. It is clear that the non-dimensional amplitude is in inverse proportion with  $S_t^2$  and  $S_c$  for the simple linear model

### 2.1 Prediction for higher-mode's VIV

The existing method for predicting higher-mode vortex-induced vibration remains mainly the use of section model wind tunnel tests while some attempts have been made to use full aeroelastic models (Fujino and Yoshida 2002). In section model tests, the prediction of lock-in wind velocity as well as vertical vibration amplitude for every possibly-excited mode bases its theoretical foundation on Eq. (6). In more detail, section model wind tunnel tests are carried out for a particular vertical mode to obtain lock-in wind velocity and the maximum amplitudes, 'lock-in' velocity and maximum amplitudes for the remaining modes are derived from Eq. (6). The procedure is as follows.

(1) Conduct section model wind tunnel tests for one particular mode  $P$  to determine the  $S_t$  number, lock-in range and maximum vibration amplitude  $\eta_P$  for that mode.

(2) Assume  $S_t$  is constant for different vertical modes and calculate the wind velocity of vortex-induced vibration for remaining modes, for example the mode  $Q$ , as follows

$$V_Q = V_P \cdot \frac{f_P}{f_Q} \quad (7)$$

where  $V_P$  may be the onset wind velocity of vortex-induced vibration, wind velocity interval of vortex-induced vibration and wind velocity of vortex-induced vibration with maximum vibration amplitude.

(3) If the modal damping ratios are the same for all modes, it is obvious that  $\eta$  is in inverse proportion with the equivalent modal mass  $m$ . As such, the relationship of vibration amplitude between mode  $P$  and mode  $Q$  is given as

$$\eta_Q = \eta_P \cdot \frac{m_P}{m_Q} \quad (8)$$

where  $m_P$  and  $m_Q$  are the equivalent modal mass for the modes  $P$  and  $Q$ . Since the mode shape for different vertical modes is very close to a sinusoidal one for suspension bridges, in particular for single-span suspension bridges, it is worthy of noting that the equivalent modal masses for different vertical modes will essentially be the same. Eq. (8) is only valid for the simple linear model of vortex-shedding force, and may become invalid for the empirical linear model of Simiu-Scanlan type if  $Y_1$  and  $Y_2$  are non-trivial.

(4) Consider further correction of vibration amplitude given by Eq. (8) in consideration of the three-dimensional mode shape as well as the span-wise correlation of vortex-shedding forces. One noticeable example of this kind of correction is the correlation length method developed by Ruscheweyh which has been included in the Eurocode (Eurocode 2005). However, Ruscheweyh's method is suitable for chimneys and other vertical structures. Chimneys may experience vortex-induced vibration for the first or second modes, which differs appreciably from higher modes of suspension bridges. Investigation on span-wise correlation of vortex-shedding forces under the higher modes vortex-induced vibration is very rare if not none.

Some investigations are underway to develop method for predicting VIV vibration amplitudes for higher modes of suspension bridges. Some key issues needing further research are summarized as follows:

- (1) Variation of  $St$  number with vibration frequency for the same model;
- (2) Variation of VIV amplitude with vibration frequency for the same  $Sc$  number;
- (3) Effect of aerodynamic damping on VIV for different modes;
- (4) Span-wise correlation of vortex-shedding forces under different mode shapes.

The first two issues will be investigated with the section models test as described in this study. The limitation of two-dimensional flow condition in section model tests excludes the three-dimensional effect of mode shapes and span-wise correction of vortex-induced lift forces, which need to be addressed with aeroelastic models (Chen *et al.* 2013). In the following, section model with the same side ratio of  $B/D=6$  but two different length scales are used to investigate the characteristics of higher-mode vortex-induced vibration for long-span suspension bridges. The models are elastically mounted with a variety of spring constants to simulate different modes of vibration in a suspension bridge.

### 3. Wind tunnel experiments

As a first step for studying the higher-mode vortex-induced vibrations, two rectangular section models having the same side ratio of  $B/D=6$  but different length scales are elastically mounted by springs with varying stiffness constants to simulate different vertical modes of vibration in suspension bridges. The wind tunnel tests are conducted in the high-speed test section of HD-2 wind tunnel at the Hunan University, the dimension of the test section is 3 m(W)×2.5 m(H)×17 m(L).

### 3.1 Sectional model and experimental setup

The side ratio of both section models is 6, and the length of both the models is 1.54 m. The two section models are denoted as A and B. The model A has a height of 12 cm and a width of 72 cm while the model B has a height of 6.7 cm and a width of 40 cm. The inner part of the model is constructed with metal materials to have sufficient rigidity while the surface of the model is covered with ABS plates to ensure the smoothness of the surface. Large end plates are connected at both ends of model to assure the two-dimensionality of the flow condition or reduce the end effect. If allowed, the ratio of model length to its width should be as large as possible; a minimum value may be 2.5 in the case of limited size of wind tunnel and preferably exceeds 5. The flow around the both model ends may be largely three-dimensional for short section models. As shown in Fig. 1, the model is elastically mounted in wind tunnel by coil springs, and the model may move in vertical and torsional directions but the motion in along-wind direction is restrained by a long steel wire. The free-stream wind velocity is recorded by Cobra probe at 1.5 m ahead of the model. The model displacements at upstream and downstream locations are measured by two laser displacement transducers, the model accelerations at upstream and downstream locations are monitored by two micro-accelerometers. The test is conducted in smooth flow ( $Iu < 1\%$  for  $U > 3$  m/s) and only zero wind attack angle is considered.

### 3.2 Data processing

The data are recorded after the model vibration become stable. The sampling frequency is 100Hz and sample duration exceeds 45s for each record. For each test case, the wind velocity, two accelerations and two displacements are measured. The two displacements  $u_1(t)$  and  $u_2(t)$  (or accelerations) are used to calculate the vertical and torsional displacements, as follows.

$$h(t) = \frac{1}{2}(u_1(t) + u_2(t)) \quad \alpha(t) = \frac{1}{a}(u_1(t) - u_2(t)) \quad (9)$$

where  $a$  is the distance between two measurement points of laser transducers.

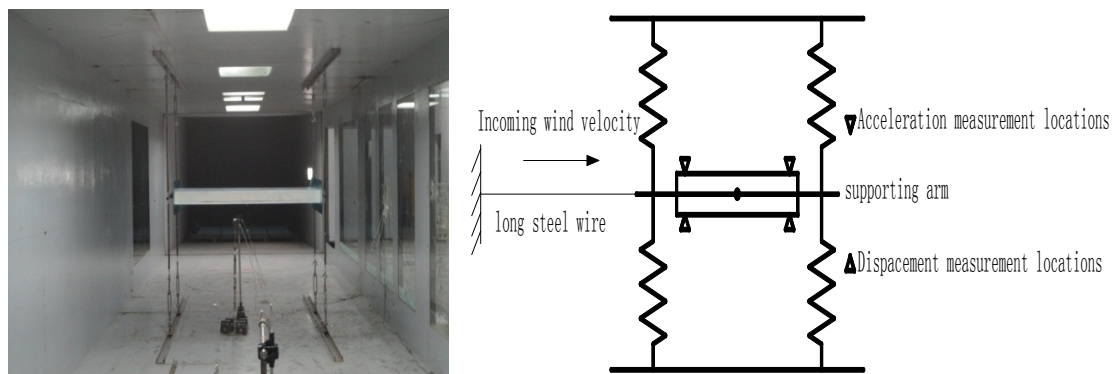


Fig. 1 Elastically-mounted section model and its supporting frames

### 3.3 Experimental results

A total of 11 cases are tested with different vibration frequencies of the section models, 8 of them for the model A and the remaining for the model B. The experimental parameters of each case for the model A and the model B are summarized in Tables 1 and 2. It is noted that each column in Table 1 are given in ascending manner of vertical frequency. Although attempts have been made to keep the total mass of the mass-spring system unchanged as much as possible for each test, the use of different springs inevitably introduces small changes of total mass. In order to eliminate this effect, the equivalent modal mass for each case are precisely calculated based on finite element modal analysis of the free vibration system consisting of rigid section model, springs, connecting arms and long steel-wire, as shown in Fig. 2. It should be pointed out that to have an observable VIV phenomenon, the Scruton number must be low, and the model natural frequency must be sufficiently high to reach the desired velocity conditions at a wind speed with small turbulence intensity.

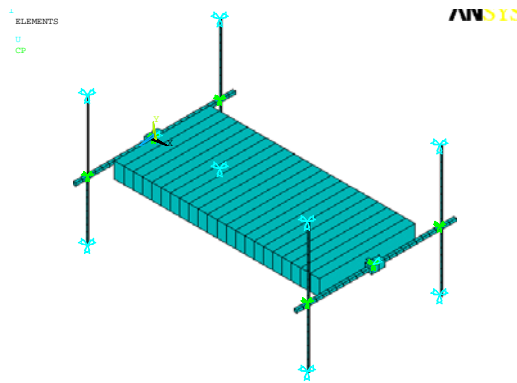


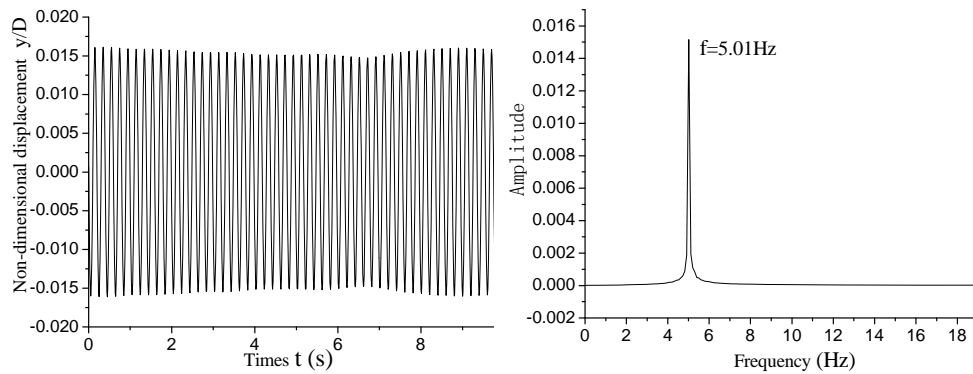
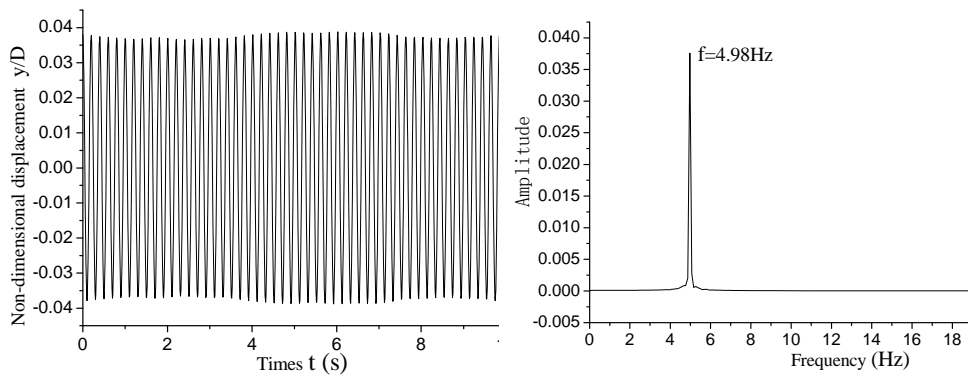
Fig. 2 Dynamic modal analysis of section model elastically mounted with test rig

Table 1 Experimental parameters for the model A

Test case	6	1	7	2	8	3	4	5
Vertical frequency $f_V$ (Hz)	2.25	2.44	2.95	3.34	3.96	4.95	5.86	6.98
Vertical damping ratio (%)	0.16	0.25	0.16	0.25	0.16	0.25	0.25	0.25
Total physical mass (Kg)	21.0	19.4	22.3	20.6	21.5	19.9	23.0	22.2
Equivalent modal mass (Kg)	18.9	17.7	18.8	18.0	18.3	17.7	18.6	18.1
$Sc$ number	1.32	1.63	1.31	1.66	1.28	1.63	1.71	1.67
Torsional frequency $f_T$ (Hz)	5.27	4.54	7.03	6.10	10.55	9.16	10.4	12.6
Torsional damping ratio (%)	0.31	0.43	0.30	0.42	--	--	--	--
$f_T/f_V$	2.34	1.86	2.38	1.83	2.66	1.85	1.77	1.81

Table 2 Experimental parameters for the model B

Test case	9	10	11
Vertical frequency $f_V$ (Hz)	2.42	3.54	5.03
Vertical damping ratio (%)	0.19	0.25	0.25
Total physical mass (Kg)	9.67	10.20	10.89
Equivalent modal mass (Kg)	7.63	8.16	7.89
$Sc$ number	1.71	2.41	2.33
Torsional frequency $f_T$ (Hz)	5.08	7.52	9.57
Torsional damping ratio (%)	0.26	0.29	0.26
$f_T/f_V$	2.10	2.12	1.90

Fig. 3 Typical vertical vortex-induced vibration at reduced velocity  $Ur=U/fD=6.58$ Fig. 4 Typical vertical vortex-induced vibration at reduced velocity  $Ur=U/fD=14.43$

Wind tunnel experiments for the 1st~5th cases of the model A are first carried out and the damping in vertical direction is 0.25%. Figs. 3 and 4 illustrate the typical near-resonance vertical vortex-induced vibration at the reduced wind velocity of 6.58 and 14.43 respectively, for the case 3. It is seen that the amplitude-frequency diagram is characterized by a peak frequency close to natural vertical frequency of the model.

Two vertical 'lock-in' ranges and two torsional 'lock-in' ranges are observed with increasing wind velocity. The torsional 'lock-in' ranges tend to diminish or become insignificant for large spring constants, which may be attributed to excessive damping in torsional direction. Fig. 5 shows the variation of the non-dimensional vertical displacement  $y/D$  with reduced velocities. As seen in Fig. 5, the first vertical 'lock-in' range for the five cases are very similar; the second vertical 'lock-in' range for the 3rd~5th cases are very similar but differs from those for the first two cases. The anomaly in the second vertical 'lock-in' for the first two cases is probably caused by the simultaneous occurrence of vertical and torsional vibration such that vertical responses transits into torsional responses. In order to validate this assumption, three additional cases with larger torsional-to-vertical frequency ratios are tested. It is observed that the second vertical 'lock-in' range for the 6th~8th cases is very similar to those of the 3rd~5th cases, as will be shown later. Therefore the experimental results from the first two cases are excluded from further analysis.

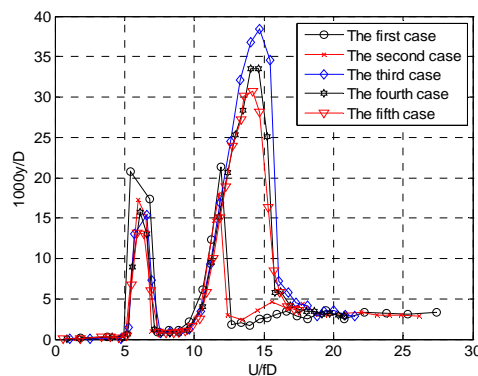


Fig. 5 Variation of the non-dimension vertical amplitude for the model A

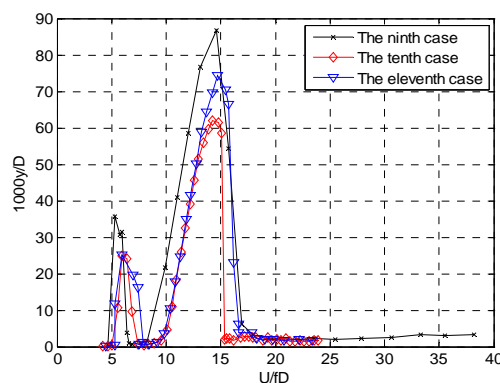


Fig. 6 Variation of the non-dimension vertical amplitude for the model B

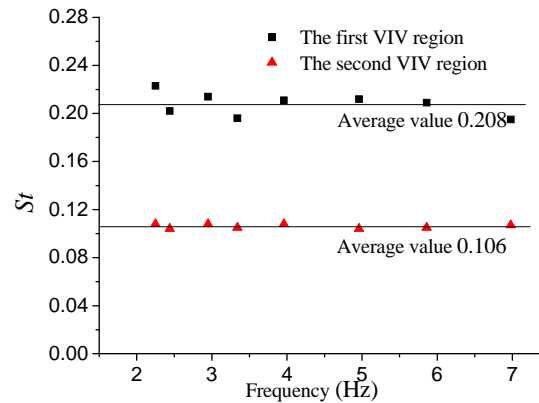


Fig. 7 Variation of  $St$  number with different frequency

Wind tunnel experiments for the model B are conducted for the 9th~11th cases. Due to the large torsional-to-vertical frequency ratio, vertical ‘lock-in’ range and torsional ‘lock-in’ range are well separated. The results of vertical ‘lock-in’ range for model B are shown in Fig. 6.

### 3.4 Analysis and discussion

(1) There are two obvious vertical ‘lock-in’ ranges for all the cases of the model A and the model B. The  $St$  number for all the 11 cases are calculated from onset velocity for the two vertical ‘lock-in’ ranges. The average value of  $St$  number for the first and the second ‘lock-in’ ranges are 0.208 and 0.106, respectively, and their stand deviation is 0.01 and 0.003. It is concluded that  $St$  numbers of the first and second vertical ‘lock-in’ ranges are almost the same for all the cases. Vibration frequency and length scale of the model have neglectible effects on  $St$  number. Therefore it is reasonable and of sufficient accuracy to derive the onset wind velocity of VIV for different modes by taking  $St$  as constant. The second vertical ‘lock-in’ range gives larger amplitude, and is therefore regarded as the excitation due to the main vortex shedding frequency. Thus the  $St$  number is 0.106 which is the same as the value given in Eurocode 1 (2005).

(2) The phenomenon of two vertical ‘lock-in’ ranges have been reported and discussed widely in the literature (e.g., Bishop and Hassan 1964, Durgin *et al.* 1980, Diana *et al.* 2006, Wu and Kareem 2012), which is mainly attributed to nonlinear nature of vortex-induced lift forces. For the present study, the second ‘lock-in’ range at higher reduced velocity is induced by the conventional vortex shedding, and the proximity of the vortex shedding frequency to model vibration frequency leads to vortex-induced resonance. The first ‘lock-in’ range may be caused by super-harmonic resonance as the vortex shedding frequency is about half of the model frequency.

(3) The mass  $m$  and damping ratio  $\zeta$  vary slightly for all the cases, and therefore the corresponding  $Sc$  number will be slightly different, as shown in Tables 1 and 2. In order to eliminate the effect of  $Sc$  number on vibration amplitude, the  $Sc$  number for the 6th case is taken as reference value, and vibration amplitude for other cases of the model A are normalized with respect to the 6th case. As the vibration amplitude is inversely proportional to  $Sc$  number, the  $Sc$ -corrected non-dimensional vibration amplitude for all other cases is calculated as

$$|\eta|'_n = |\eta|_n \cdot \frac{S_{cn}}{S_{c6}} \tag{10}$$

where the subscript  $n$  represent the case  $n$ ;  $|\eta|'_n$  is the  $Sc$ -corrected vibration amplitude. The variations of  $Sc$ -corrected vibration amplitude for the model A are show in Fig. 8. After correction, the discrepancy in vibration amplitude is further reduced for the model A. Fig. 9 shows the  $Sc$ -corrected vibration amplitude for the model B where the 9th case is taken as reference. Both Figs. 8 and 9 imply that vibration frequency does not have important effects on vibration amplitude. It may be concluded the assumption that the non-dimensional vibration amplitudes for different vertical modes is the same is valid provided that the  $Sc$  number is the same for different modes.

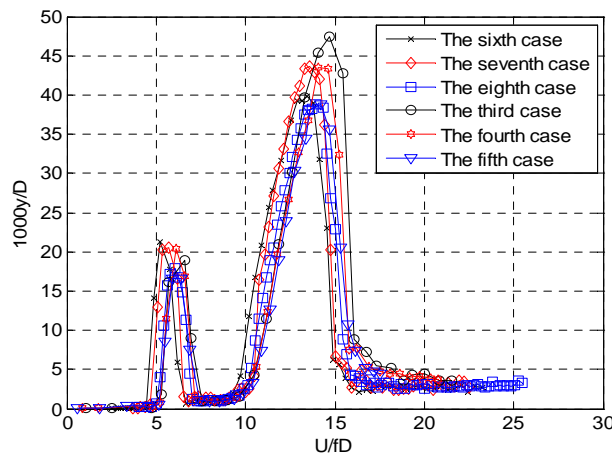


Fig. 8  $Sc$ -corrected amplitude for model A

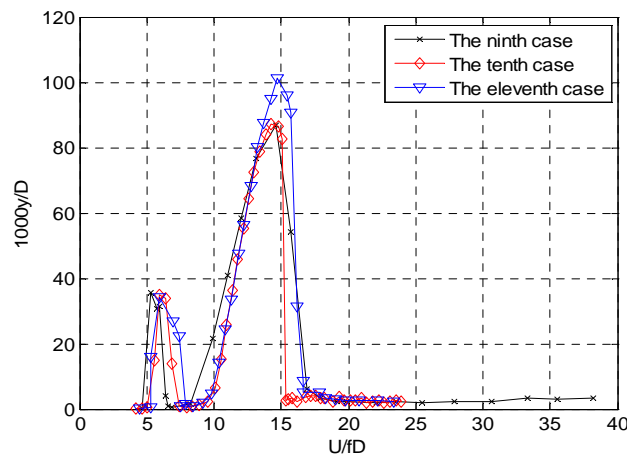


Fig. 9  $Sc$ -corrected amplitude for model B

#### 4. Conclusions

Two rectangular section models with the same side ratio of  $B/D=6$  but different length scales have been used to investigate the variation of  $St$  number and VIV amplitude with modal frequency. It is shown that (1) two vertical ‘lock-in’ ranges develop for all the cases and  $St$  number in each vertical VIV remains constant for different vibration frequencies, implying  $St$  does not rely on the model frequency or  $Re$  number, at least for the studied rectangular section; (2) more importantly the VIV amplitude at different vibration frequencies are almost the same for the same model scale provided that the  $Sc$  number is the same; (3) the second ‘lock-in’ ranges is induced by the conventional vortex shedding, while the first ‘lock-in’ may be caused by the super-harmonic resonance.

As the section model is used in this study, the presented results confine themselves to the two-dimensional flow conditions. A novel aeroelastic model has been developed to study the three-dimensional effect of both mode shape and flow conditions for higher mode vortex-induced vibrations, and some of these investigation are underway (Chen *et al.* 2013).

#### Acknowledgments

The work is supported by the Natural Science Foundation of China (NSFC Nos. 51278189, 51422806, and 91215302), which are greatly acknowledged

#### References

- Barrero-Gil, A. and Fernandez-Arroyo P. (2013), “Maximum vortex-induced vibration of a square prism”, *Wind Struct.*, **16**(4), 341-354.
- Bearman, P.W. (1984), “Vortex shedding from oscillating bluff bodies”, *Annu. Rev. Fluid Mech.*, **16**, 195-222.
- Bishop, R.E.D. and Hassan, A.Y. (1964), “The lift and drag forces on a circular cylinder in a flowing fluid”, *P. Roy. Soc. London. Series A: Math. Phys. Sci.*, **277**, 32-50.
- Borna, A., Habashi, W., McClure, G. and Nadarajah, S.K. (2013), “CFD-FSI simulation of vortex-induced vibrations of a circular with low mass-damping”, *Wind Struct.*, **16**(5), 411-431.
- Chen, Z.Q., Chen, W., Hua, X.G. and Huang, Z.W. (2013), “High-mode’s vortex induced vibration Part II: aeroelastic model study”, *Proceedings of the 7th European and African Conference on Wind Engineering*, July 2013, Cambridge, UK.
- Diana, G., Resta, F., Belloi, M. and Rocchi, D. (2006), “On the vortex shedding forcing on suspension bridge deck”, *J. Wind Eng. Ind. Aerod.*, **94**(5), 341-363.
- Durgin, W.W., March, P.A. and Lefebvre, P.J. (1980), “Lower mode response of circular cylinders in smooth flow”, *J. Fluid Eng. - T ASME*, **102**, 183-190.
- Eurocode 1 EN 1991-1-4 (2005), Actions on structures – Part 1-4: General actions – Wind actions, European Standard EN 1991-1-4:2005.
- Fujino Y. and Yoshida Y. (2002), “Wind induced vibration and control of Trans-Tokyo Bay Crossing Bridge”, *J. Struct. Eng. - ASCE*, **128**(8), 1012-1025.
- Larsen, A., Esdahl, S., Andersen, J.E. and Vejrum, T. (2000), “Storebalt suspension bridge-vortex shedding excitation and mitigation by guide vanes”, *J. Wind Eng. Ind. Aerod.*, **88**, 283-296.
- Li, H., Laima, S., Ou, J.P., Zhao, X.F., Zhou, W.S., Yu, Y. and Li, N. (2011), “Investigation of vortex-induced vibration of a suspension bridge with two separated steel box girders based on field

- measurements”, *Eng. Struct.*, **33**, 1894-1907.
- Sarpkaya, T.A. (2004), “Critical review of the intrinsic nature of VIV”, *Fluid Mech. Appl.*, **75**, 159-161.
- Scruton, C. and Flint, A.R. (1964), “Wind-excited oscillations of structures”, *Proc. Inst. Civil Engineers*, **27**(4), 673-702.
- Simiu, E. and Scanlan, R. H. (1996), *Wind Effects on Structures: Fundamentals and Applications to Design*, 3rd edition, John Wiley, New York
- Yi, T.H., Li, H.N. and Zhang, X.D. (2012), “A modified monkey algorithm for optimal sensor placement in structural health monitoring”, *Smart Mater. Struct.*, **21**(10), 1-9.
- Williamson, C.H.K. and Govardhan, R. (2004), “Vortex-induced vibrations”, *Annu. Rev. Fluid Mech.*, **36**(1), 413-455.
- Wu, T. and Kareem, A. (2012), “An overview of vortex-induced vibration (VIV) of bridge decks”, *Front. Struct. Civil Eng.*, **6**(4), 335-347.